Direct Observation of Percolation in a Manganite Thin Film

Liuwan Zhang,[1]*† Casey Israel,[1]* Amlan Biswas,[2]‡ R. L. Greene,[2] Alex de Lozanne[1]§

Upon cooling, the isolated ferromagnetic domains in thin films of $La_{0.33}Pr_{0.34}Ca_{0.33}MnO_3$ start to grow and merge at the metal-insulator transition temperature T_{P1}, leading to a steep drop in resistivity, and continue to grow far below T_{P1}. In contrast, upon warming, the ferromagnetic domain size remains unchanged until near the transition temperature. The jump in the resistivity results from the decrease in the average magnetization. The ferromagnetic domains almost disappear at a temperature T_{P2} higher than T_{P1}, showing a local magnetic hysteresis in agreement with the resistivity hysteresis. Even well above T_{P2}, some ferromagnetic domains with higher transition temperatures are observed, indicating magnetic inhomogeneity. These results may shed more light on the origin of the magnetoresistance in these materials.

Colossal magnetoresistive materials of the type $R_{1-x}A_xMnO_3$ (*1*, *2*) (R is a trivalent rare-earth ion and A is a divalent dopant) have been extensively studied in past years because of their value in fundamental physics and their potential applications. For a wide doping range around $x = 1/3$, these materials exhibit the colossal magnetoresistance (CMR) effect, a large resistance drop with the application of a magnetic field. These materials show an insulator–metal transition from a high-temperature insulating phase to a low-temperature metallic phase characterized by a peak at T_P in the resistivity versus temperature curve. This phase transition is accompanied by a magnetic transition from a high-temperature paramagnetic phase to a low-temperature ferromagnetic (FM) phase at the Curie temperature, T_C. These phase transitions are interpreted in terms of the double exchange (DE) interaction model (*3*). The doping of A^{2+} ions in R^{3+} sites results in a mixed Mn^{3+}/Mn^{4+} valence. Electrons in the e_g orbital can hop from the Mn^{3+} to the neighboring Mn^{4+} sites with strong on-site Hund's coupling through the O^{2-} in between. The motion of the electrons is enhanced in the FM state when the core Mn d-shell spins are parallel. In turn, the hopping electrons promote FM order because they tend to preserve their spin directions. The applied magnetic field can suppress their spin disorder around T_C, shifting both T_C and T_P to higher temperatures, leading to the CMR effect. However, the DE mechanism alone is not sufficient to describe the high-temperature transport properties and to quantitatively explain the CMR. Therefore, some other mechanisms such as electron-phonon coupling (*4*) due to local Jahn-Teller distortions at the Mn^{3+} sites and orbital ordering effects (*5*) must be considered. All these driving mechanisms conspire to produce a very complex phase diagram as a function of the composition, x, with as many as seven different regions (*4*). Many of the neighboring phases have similar ground-state energies; consequently, the phase boundaries can be readily displaced by perturbations such as the application of a magnetic field (*6*), of mechanical or structural pressure (*7*), or by chemical substitutions (*8*). This latter possibility is interesting because it has been shown to result in large-scale electronic phase separation and to produce hysteretic behavior in the transport properties.

Indeed, there is growing experimental and theoretical evidence that the doped manganites are inhomogeneous and that phase separation is common in these materials (*9*, *10*). Uehara *et al.* (*8*) studied the $La_{5/8-x}Pr_xCa_{3/8}MnO_3$ system using electron microscopy. They found that at low temperatures, below T_P, the system is electronically phase-separated into a submicrometer-scale mixture of insulating regions and metallic FM domains, although they could not characterize the local magnetic properties of these domains. They explained the CMR effect by percolative transport through the FM domains. We present the direct observation of the formation of these percolative networks as the sample is cooled, and their disappearance upon warming, but at a higher temperature, by directly measuring the temperature-dependent local magnetic microstructure in $La_{0.33}Pr_{0.34}Ca_{0.33}MnO_3$ thin films using a low-temperature (LT) magnetic force microscope (MFM). An unexpected finding is that the magnetic domains continue to grow and change at low temperatures upon cooling and that upon warming they still exist at temperatures above T_{P2}.

Our homemade LT-MFM (*11*) and its use to image CMR thin films (*12*) have been described before except that the homemade electronics have been replaced by a Nanoscope IIIa controller from Digital Instruments (*13*). We used the LiftMode scanning mode that has two interleaved scan processes. The first pass is a frequency-modulated TappingMode atomic force microscope scan, from which the topography is obtained. The next pass is a frequency-modulated LiftMode scan, in which the tip-sample distance is increased by 100 nm. The MFM image is formed by changes in the resonant frequency of the lever during the LiftMode scan. We used noncontact Piezolevers (*14*) with resonant frequency of about 110 kHz. The tip is made sensitive to the magnetic force by depositing a 50-nm-thick Fe film on one side and magnetizing it along its axis. The scan size was calibrated at different temperatures by scanning a sample with known periodic features.

The domain patterns imaged by MFM of CMR films with different easy axes have different shapes (*15*). MFM images of our sample indicate an in-plane easy axis. Because the MFM is sensitive to force gradients perpendicular to the sample, in order to see clearly the domains instead of the domain walls, a perpendicular magnetic field is needed to partially align the magnetization of the domains out of plane. In the case of the cooling sequence, the tip itself provides this cooling field. For warming images we first cooled the sample across T_{P1} to a low temperature in a 25-G magnetic field perpendicularly applied to the whole sample, then turned off the field to start scanning during warming. The thermal drift of the tip position relative to the sample was compensated for during image acquisition with x-y offsets of the scan piezo and z offsets of the coarse approach mechanism to follow the same area of the sample. The latter precludes us from scanning the same area of the sample when changing from cooling to warming, because a change in the direction of the coarse approach mechanism causes an unpredictable change in the lateral position of the sample. The temperature change rate was 0.1 K/min during scanning (*16*).

---

[1] Department of Physics, University of Texas, Austin, TX 78712, USA. [2] Center for Superconductivity Research, Department of Physics, University of Maryland, College Park, MD 20742, USA.

*These authors contributed equally to this work.

†Permanent address: Department of Physics, Tsinghua University, Beijing 100084, People's Republic of China.

‡Present address: Department of Physics, University of Florida, Gainesville, FL 32611–8440, USA.

§To whom correspondence should be addressed. E-mail: lozanne@physics.utexas.edu

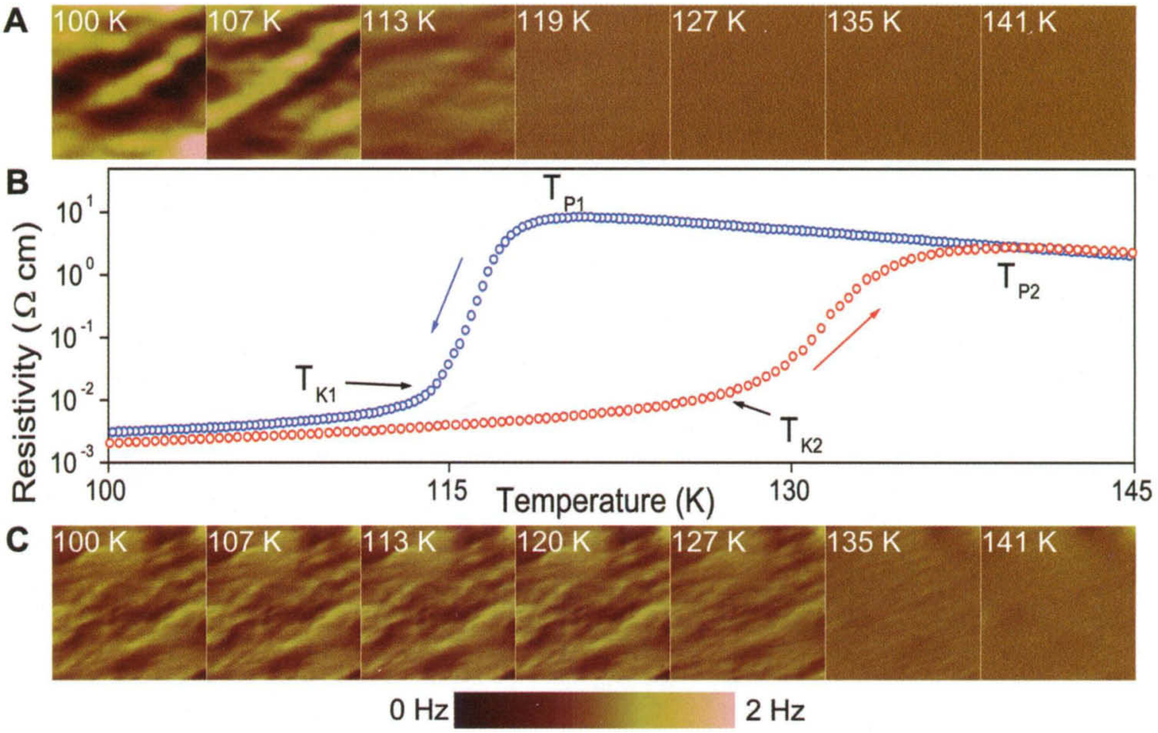

Fig. 1. The temperature-dependent MFM image sequence (**A**) for cooling and (**C**) for warming, and the resistivity (**B**) of the $La_{0.33}Pr_{0.34}Ca_{0.33}MnO_3$ thin film over a thermal cycle. The blue series corresponds to cooling, the red series to warming. The center of each image is aligned horizontally with the temperature scale from (B) at the time of image capture. Scanned areas are 6 μm by 6 μm for all cooling images and 7.5 μm by 7.5 μm for all warming images. All cooling images were taken at one area of the sample, and all warming images were taken at another area. See Movies S1 to S4 for the complete image sequences.

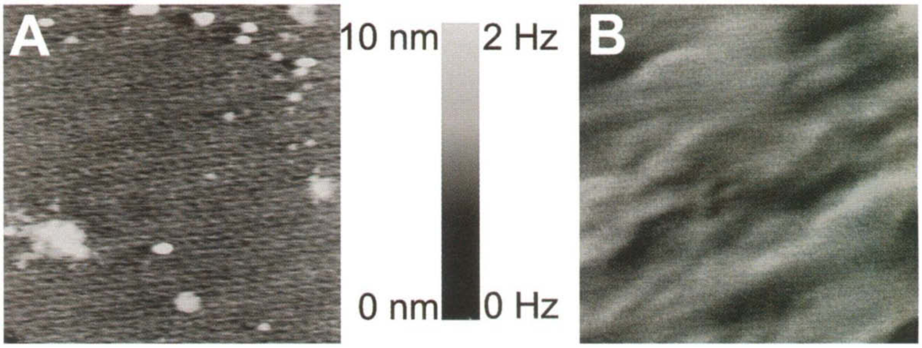

Fig. 2. (**A**) Topography image and (**B**) the corresponding MFM image recorded on the same area (7.5 μm by 7.5 μm) of the sample at 120 K during warming.

The films were grown on $NdGaO_3$ (NGO) (110) substrates by pulsed laser deposition to a thickness of 60 nm. They were grown in an oxygen atmosphere of 400 mTorr at a rate of about 1 Å/s while the substrate temperature was 820°C. The temperature dependence of the resistivity of the film (Fig. 1B) shows that on cooling from room temperature, the resistivity gradually increases, attaining a maximum at T_{P1} = 120 K. This is followed by a steep resistivity drop to the knee temperature T_{K1} = 114 K, and then slow changes to 4.2 K. On warming, the resistivity follows the cooling curve at first, then deviates to lower resistivity values. After an abrupt jump beginning at the warming knee temperature T_{K2} = 128 K, the resistivity reaches a maximum at T_{P2} = 140 K, and finally coincides with the cooling curve at high temperature. T_{P2} is 20 K higher than T_{P1}, showing a pronounced hysteresis typical of a first-order phase transition. The resistivity values are similar to those of single crystals of these compounds (*17*), but the transition widths are much narrower for our thin films (about 8 to 9 K). Unfortunately, the magnetization of these 60-nm films on NGO is difficult to measure owing to the paramagnetism of the substrate (*18*).

Figure 2 shows a typical topographic image and its corresponding MFM image well below T_{P2}. Comparison of the two images indicates that the main features in the MFM image have no counterparts in the topography image. The features in the MFM image are due to the nonuniform magnetic field distribution and are therefore domains of differing magnetization. As the microscale FM domains form around T_{P1}, the field-cooling process tends to align some component of their magnetizations out of plane in the direction of the field. The interaction between the tip and these aligned domains is then attractive and lowers the resonant frequency of the cantilever relative to that of the rest of the sample. The MFM image is a record of these shifts in the resonant frequency. Thus, the dark regions are FM metallic regions with magnetization more parallel to the tip moment than that of the bright regions. This is further supported by growth of the dark regions at low temperature.

The MFM images taken during cooling at one area and warming at another area are displayed in Fig. 1 (*19*) (see more detail in Movies S1 to S4). During the cooling process the MFM images are nearly uniform above T_{P1}. Just below T_{P1}, the contrast starts to appear. The contrast of the sequence is gradually enhanced with decreasing temperature, indicating that the magnetization of the FM domains becomes increasingly stronger. Just past T_{K1} the percolation of the FM domains is clearly seen. When the temperature is decreased further, although the change in the resistivity is smaller, the contrast of the image continues to increase and the FM domains merge and enlarge, which is an unexpected result.

However, during warming below T_{K2}, both the contrast and the size of the FM regions are nearly unchanged. Above T_{K2}, although the size of the FM regions is constant, the contrast rapidly decreases. At T_{P2} the contrast almost completely disappears. The local magnetic hysteresis is consistent with the resistivity hysteresis and qualitatively consistent with the magnetization measurement on polycrystalline samples with similar composition (*20*).

The FM domains in the warming images

have a much smaller size than the cooling images at the same temperatures below T_{K1}. This difference may be due to the way in which the sample is cooled. The tip of the MFM vibrates above the sample surface at the lever's resonant frequency of 110 KHz, contacting the sample at the lowest point of each oscillation. At this contact point, the magnetic field applied by the tip is large (10^2 to 10^3 G) (*21*). Roughly, as the tip is scanned, a strong periodic magnetic pulse with a frequency of 110 KHz is scanned over the sample. We believe that upon cooling, although this scanning high-frequency localized magnetic pulse may not change the relative FM fraction (*22*), it can partially align the magnetization of the domains and drive the motion of the domain walls, leading to the merging and enlargement of the domains. On the other hand, the warming images were obtained after the sample was cooled to the lowest temperature in a magnetic field of 25 G. During this cooling process, the tip is far away from the sample. This cooling field may not be strong enough to move the domain walls. When scanning during warming, the domain walls are strongly pinned. As a result, the shape of the domains is unchanged. As T_{P2} is approached, the average magnetization decreases, which results in a rise in the resistivity (Fig. 1B) (*23*). Our observations indicate that during cooling, the percolation of the FM domains causes the steep resistivity drop, whereas during warming, the FM conductive paths remain until near T_{P2}, but the decrease in the average magnetization leads to the jump in resistivity. This also may explain why the knee in the resistivity is sharper during cooling than during warming.

Below T_{K1} the enlargement of the domains is mainly due to the merging of the domains, and not to the increase of the FM volume fraction. Therefore, the resistivity changes slowly below T_{K1}, as shown in Fig. 1B.

Even well above T_{P2}, there is still a slight but discernable contrast in some areas, which can be more clearly seen in the supplemental movies. We propose that this is due to the magnetic inhomogeneity above T_P that is frequently observed in similar CMR materials (*24–26*).

Owing to the constraining effect of the substrate, some effects observed in bulk samples may be suppressed or different for these thin films (*17*). This might account for the sharper transitions in the thin films and the narrower hysteresis regions. This implies that the temperature-dependent magnetic microstructure in thin films may be modified due to the effect of the substrate.

References and Notes

1. R. von Helmot, J. Wecker, B. Hopzapfel, L. Schulz, K. Samwer, *Phys. Rev. Lett.* **71**, 2331 (1993).
2. S. Jin *et al.*, *Science* **264**, 413 (1994).
3. C. Zener, *Phys. Rev.* **82**, 403 (1951).
4. A. J. Millis, *Nature* **392**, 147 (1998).
5. R. Maezono, S. Ishihara, N. Nagaosa, *Phys. Rev. B* **58**, 11583 (1998).
6. A. Asamitsu, Y. Moritomo, Y. Tomioka, T. Arima, Y. Tokura, *Nature* **373**, 407 (1995).
7. C. Martin *et al.*, *Eur. Phys. J. B* **16**, 469 (2000).
8. M. Uehara, S. Mori, C. H. Chen, S. W. Cheong, *Nature* **399**, 560 (1999).
9. M. B. Salamon, M. Jaime, *Rev. Mod. Phys.* **73**, 583 (2001).
10. N. D. Mathur, P. B. Littlewood, *Solid State Commun.* **119**, 271 (2001).
11. C. W. Yuan, E. Batalla, A. de Lozanne, M. Kirk, M. Tortonese, *Appl. Phys. Lett.* **65**, 1308 (1994).
12. Q. Lu, C. Chen, A. de Lozanne, *Science* **276**, 2006 (1997).
13. Materials and methods are available as supporting material on *Science* Online.
14. Park Scientific Instruments (now Veeco Instruments), Santa Barbara, CA.
15. R. Desfeux, S. Bailleul, A. Da Costa, W. Prellier, A. M. Haghiri-Gosnet, *Appl. Phys. Lett.* **78**, 3681 (2001).
16. We recorded another set of cooling and warming images using a temperature change rate of 0.3 K/min. The temperature-dependent evolution of the FM domains is qualitatively the same as that of the sets shown in the text. We believe that our observation is largely due to the temperature change and not time relaxation.
17. V. Podzorov, B. G. Kim, V. Kiryukhin, M. E. Gershenson, S.-W. Cheong, *Phys. Rev. B* **64**, 140406 (2001).
18. A. Biswas *et al.*, *Phys. Rev. B* **61**, 9665 (2000).
19. We emphasize that all of our sets of cooling and warming images obtained on different areas of the sample with different noncontact piezolevers show the same temperature-dependent evolution of domains. As described in the text, during cooling from room temperature to T_{P1}, all the images are uniform, and from low temperature to T_{K2} during warming, both the size and the contrast of the images are nearly unchanged. To maintain the consistency between the resistivity hysteresis and the micromagnetic hysteresis, we have simply reproduced the three highest temperature images in Fig. 1A and the three lowest temperature images in Fig. 1C.
20. P. Levy *et al.*, *Phys. Rev. B* **65**, 140401 (2002).
21. L. Kong, S. Y. Chou, *Appl. Phys. Lett.* **70**, 2043 (1997).
22. F. Parisi, P. Levy, L. Ghivelder, G. Polla, D. Vega, *Phys. Rev. B* **63**, 144419 (2001).
23. A. Urushibara *et al.*, *Phys. Rev. B* **51**, 14103 (1995).
24. Y.-A. Soh, G. Aeppli, N. D. Mathur, M. G. Blamire, *Phys. Rev. B* **63**, 020402 (2000).
25. ———, *J. Appl. Phys.* **87**, 6743 (2000).
26. M. Fäth *et al.*, *Science* **285**, 1540 (1999).

27. The work at Austin was supported by NSF grant DMA-0072834 and The Texas Center for Superconductivity at the University of Houston. The work at Maryland was supported in part by NSF grant MRSEC-00-80008. We thank S.-W. Cheong, N. D. Mathur, A. Guha, Q. Niu, Y. Tsui, and J. Lee for fruitful discussions and T. Ruiter (Veeco Metrology Group) for providing piezoresistive cantilevers.

Supporting Online Material
www.sciencemag.org/cgi/content/full/1077346/DC1
Materials and Methods
Movies S1 to S4

14 August 2002; accepted 9 September 2002
Published online 19 September 2002;
10.1126/science.1077346
Include this information when citing this paper.

Ideal Pure Shear Strength of Aluminum and Copper

Shigenobu Ogata,[1,2,3] Ju Li,[1,4] Sidney Yip[1]*

Although aluminum has a smaller modulus in $\{111\}\langle 11\bar{2}\rangle$ shear than that of copper, we find by first-principles calculation that its ideal shear strength is larger because of a more extended deformation range before softening. This fundamental behavior, along with an abnormally high intrinsic stacking fault energy and a different orientation dependence on pressure hardening, are traced to the directional nature of its bonding. By a comparative analysis of ion relaxations and valence charge redistributions in aluminum and copper, we arrive at contrasting descriptions of bonding characteristics in these two metals that can explain their relative strength and deformation behavior.

The minimum shear stress necessary to cause permanent deformation in a material without imperfections is fundamental to our concept of materials strength and its theoretical limits under large strains (*1*, *2*). With the possible exception of recent nanoindentation measurements (*3*), it has not been feasible to directly measure the ideal shear strength of crystals. The demonstration that this property can be reliably determined by first-principles calculations therefore would have important implications for the understanding of the behavior of solids at the limit of structural stability. Results on stress-strain behavior of Al and Cu in $\{111\}\langle 11\bar{2}\rangle$ shear, calculated with density functional theory (DFT) and accounting for full atomic relaxation, have been reported (*4*), where Cu was found to have a higher ideal shear strength than that of Al. Using various DFT methods and systematically cross-checking the results, we further investigated the shear strength and deformation of Al and Cu and found instead that Al has the higher strength. Here, we report and substantiate our findings by detailing the energetics of shear deformation, the pressure-hardening behavior, and valence charge redistribution during deformation. These considerations show that the ideal shear strength and related

---

[1] Department of Nuclear Engineering, Massachusetts Institute of Technology, Cambridge, MA 02139, USA. [2] Department of Mechanical Engineering and Systems, [3] Handai Frontier Research Center, Osaka University, Osaka 565–0871, Japan. [4] Department of Materials Science and Engineering, Ohio State University, Columbus, OH 43210, USA.

*To whom correspondence should be addressed. E-mail: syip@mit.edu